Journal of Materials Chemistry B

ROYAL SOCIETY OF CHEMISTRY

PAPER

View Article Online
View Journal | View Issue

Cite this: J. Mater. Chem. B, 2023, 11, 3387

Gold nanoparticle-based two-photon fluorescent nanoprobe for monitoring intracellular nitric oxide levels†

Carla Arnau del Valle, [a] Paul Thomas,[b] Francisco Galindo,[c] María Paz Muñoz [ad] and María J. Marín *[a]

Nitric oxide (NO) plays an important role in the regulation of the immune, cardiovascular and nervous systems. Consequently, being able to monitor and quantify intracellular NO levels would provide a greater understanding of the implications of this molecule in the different biological processes, including, for example, in cancer. Here, we report a broadly applicable two-photon excitable fluorescent nanoprobe able to detect and potentially quantify NO levels in an extensive range of cellular environments. The nanoprobe consists of a thiolated photoinduced electron transfer-based two=photon fluorescent probe attached onto the surface of 2.4 ± 0.7 nm gold nanoparticles (**DANPY-NO@AuNPs**). The nanoprobe, which can be synthesised in a reproducible manner and exhibits great stability when stored at room temperature, is able to selectively detect NO in solution, with a dynamic range up to 150 μM, and at pH values of biological relevance. **DANPY-NO@AuNPs** were able to selectively detect endogenous NO in RAW264.7γ NO^- macrophages and THP-1 human leukemic cells; and endogenous and exogenous NO in endothelial cells. The nanoprobe accumulated in the acidic organelles of the tested cell lines showing negligible toxicity. Importantly, **DANPY-NO@AuNPs** showed potential to quantify intracellular NO concentrations in MDA-MB-231 breast cancer cells. The biological evaluation of the nanoprobe was undertaken using confocal laser scanning (images and intracellular emission spectra) and multiphoton microscopies, and flow cytometry. Based on their excellent sensitivity and stability, and outstanding versatility, **DANPY-NO@AuNPs** can be applied for the spatiotemporal monitoring of *in vitro* and *in vivo* NO levels.

Received 16th January 2023,
Accepted 6th March 2023

DOI: 10.1039/d3tb00103b

rsc.li/materials-b

Introduction

Nitric oxide (NO), the primary precursor of all the intracellular reactive nitrogen species (RNS),[1] is involved in many biological processes such as signal transduction, smooth muscle relaxation, peristalsis, immune system control, neurotransmission, blood pressure modulation, learning and memory.[2] NO is also involved in the oxidation of DNA, lipids, proteins and carbohydrates; and, as a consequence, contributes to the development of pathological events such as Alzheimer's, Huntington's and Parkinson's disease, amyotrophic lateral sclerosis, cerebral ischemia, stroke, and cancer.[3–7]

Efforts have been made to develop new strategies for the detection and monitoring of intracellular NO to understand its complex metabolism. Approaches used to detect NO include fluorescence-based bioimaging, spectroscopic analysis, electrochemistry, electron spin resonance spectroscopy, chemiluminescence and colorimetry.[8,9] Despite the advances reported to date, the direct and real-time detection of NO has proven challenging due to its low concentration, short lifetime and high reactivity with several reactive oxygen species (ROS).[10] The ideal detection system should exhibit high selectivity and sensitivity towards NO with a low limit of detection (LOD), high stability and insensitivity to pH changes, high biocompatibility, high membrane permeability and photostability, and capacity to monitor a wide range of NO concentrations and in a variety of cellular systems.[11,12]

Fluorescent probes present advantages for intracellular applications including direct bioimaging detection and great

[a] School of Chemistry, University of East Anglia, Norwich Research Park, Norwich, NR4 7TJ, UK. E-mail: m.marin-altaba@uea.ac.uk
[b] Henry Wellcome Laboratory for Cell Imaging, Faculty of Science, University of East Anglia, Norwich Research Park, Norwich, NR4 7T, UK
[c] Departamento de Química Inorgánica y Orgánica, Universitat Jaume I, Av. Sos Baynat s/n, Castellón de la Plana, 12071, Spain
[d] Department of Chemistry, Lancaster University, Bailrigg, Lancaster, LA1 4YB, UK

† Electronic supplementary information (ESI) available: The experimental section of this paper and the supporting figures including NMR spectra of DANPY-NO-ligand and its intermediates; characterisation of **DANPY-NO@AuNPs** and sensitivity and selectivity characterisation; and supporting intracellular controls and further intracellular characterisation. See DOI: https://doi.org/10.1039/d3tb00103b

spatio-temporal resolution when combined with fluorescence microscopy techniques, and can be designed to exhibit excellent sensitivities, large dynamic ranges, and high specificity.[2] Considerable endeavours have been centred on the design of intracellular fluorescent NO molecular probes.[11,13–21] Amongst these, aromatic *ortho*-diamino (*o*-diamino)-fluorophore derivatives have attracted special attention and plenty of examples can be found in the literature.[22–30] Some of these *o*-diamino-derivative probes are commercially available and broadly used for the detection of NO in biological samples. For example, 4,5-diaminofluorescein (DAF-2, LOD: 5 nM) was reported by Nagano and co-workers in 1998[22,23] and its membrane permeable version, DAF-2 diacetate, is currently commercially available as a fluorescent dye for NO detection. A more photostable and sensitive (LOD: *ca.* 3 nM) probe, 4-amino-5-methylamino-2′,7′-difluorofluorescein (DAF-FM) diacetate was developed by the same authors,[24] which is also commercially available and can be used to detect NO using different instrumental techniques. However, the poor photostability and requirement of UV-Vis excitation wavelengths are some of the limitations of most of the reported examples, difficulting their application for *in vivo* detection of NO.

Current research efforts are focussing on the development of systems that can be excitable with near-infrared (NIR) light, which allows for deeper tissue penetration and minimal photodamage, and leads to negligible autofluorescence.[31] For these examples, multiphoton microscopy, which uses two NIR photons for excitation,[32] can be employed to monitor the sensing capability of the systems. In the past decade, several examples of two-photon excitable NO probes have been described in the literature, showing an improvement in the detection of NO.[33–41] Amongst them, we recently reported a highly photostable and versatile two-photon fluorescent probe, DANPY-NO, for the detection of a wide range of intracellular NO concentrations in macrophages and endothelial cells using confocal laser scanning microscopy (CLSM), multiphoton microscopy, and flow cytometry.[42]

Further developments in intracellular sensing and imaging have been achieved with the use of nanoparticles (NPs), which present advantages over molecular-based systems, including improved signal-to-noise ratios due to the high loading of sensing units on the large surface of the NP.[43] Furthermore, NPs permit the loading of multiple components on a single platform, which provides an extensive range of engineering possibilities: *i.e.* incorporation of targeting agents, ligands that render water solubility and biocompatibility, other fluorescent ligands to achieve ratiometric sensing, or drugs for theranostic applications.

Several examples of fluorescent-based nanoprobes for the detection of NO have been recently reported using organic and inorganic NPs. For example, polymeric NPs have been used for the encapsulation of fluorescent molecular NO probes.[44–47] Jin *et al.* encapsulated DAF-FM in poly(lactic-*co*-glycolic acid) NPs and used the nanoprobe for the detection of both NO released from chondrocytes, and from the joint of osteoarthritis rats.[44] Contrary to what was observed with the encapsulated probe, the free DAF-FM was not visualised after injection *in vivo* because it was rapidly diluted and distributed through the whole body. Latha *et al.* reported polyvinyl alcohol-based NPs covalently functionalised with rhodamine B for the successful detection of exogenous and endogenous NO in rabbit fibroblast-like synoviocytes.[47] Intrinsically fluorescent NPs have also been used for the development of NO nanoprobes. Bhattacharya *et al.* synthesised NO-sensitive carbon dots (CDs) that detected endogenous NO in stimulated RAW264.7 macrophages.[48] The CDs-based nanoprobe had a LOD of 80 nM and exhibited good selectivity towards NO; but showed sensitivity to pH in a broad range of pH values (2–8), which could lead to non-selective detection of NO intracellularly.[48] NO has been reported to be able to react with quantum dots (QDs) by coordination with Cd forming a NO-Cd complex which leads to a reduction of the fluorescence emission. Following this, Tan *et al.* developed biocompatible CdSe QDs stabilised with chitosan that were able to detect exogenous NO when internalised in porcine iliac artery endothelial cells.[49]

The examples listed above use UV-Vis light to perform the detection of NO with the consequent limitations. Only a few examples can be found in the literature reporting the development of NIR excitable fluorescent nanoprobes for optimal bioimaging and diagnosis.[50,51] In particular for NO nanoprobes, Kim *et al.* reported single-walled carbon nanotubes modified with 3,4-diaminophenyl-functionalised dextran that were used for the detection of endogenous and exogenous NO in RAW264.7 cells using NIR excitation; and showed the potential to penetrate mouse tissue and to detect NO *in vivo*.[52] More recently, other authors have described the potential of the NIR excitable upconverting NPs for the quantification of intracellular NO.[53,54]

Amongst the different types of NPs, gold NPs (AuNPs) have shown excellent potential for chemical and biological sensing applications.[55–64] In particular for the detection of NO, Leggett *et al.* developed a NO biosensor based on AuNPs functionalised with fluorescently tagged cytochrome *c* that was able to detect, using CLSM, endogenous and exogenous NO in RAW264.7 cells, and NO produced by the cells during bacterial phagocytosis.[58] However, to the best of our knowledge, the potential of using two-photon excitable AuNPs-based systems to detect NO in a broad range of intracellular environments has not been explored to date. These two-photon excitable AuNPs-based platforms could contribute to a better understanding of the intracellular role of NO permitting deeper tissue penetration. Furthermore, they could be further functionalised yielding NO ratiometric nanoprobes or theranostic nanosystems.

Given the excellent performance of the two-photon excitable NO probe, DANPY-NO, recently reported by our group,[42] and our successful application of AuNPs-based systems for the detection and quantification of analytes of intracellular interest,[58,64,65] the work described here reports the first example of a two-photon nanoprobe based on AuNPs (**DANPY-NO@AuNPs**, Fig. 1(a)) for the intracellular detection and potential quantification of NO that has been proven suitable to work in a broad range of cellular environments. The **DANPY-NO@AuNPs** showed good sensitivity towards NO with a LOD of

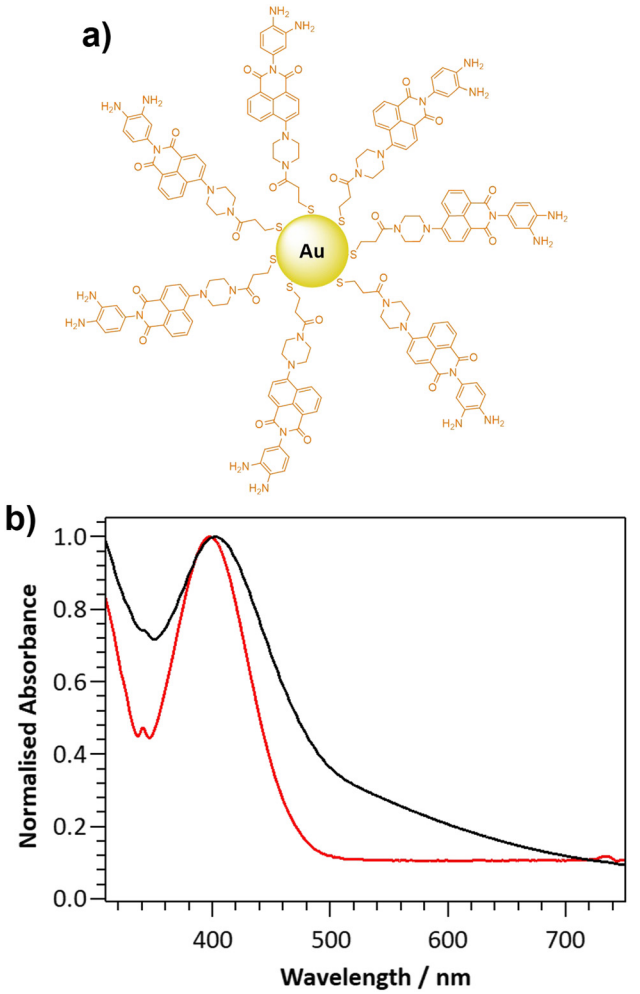

Fig. 1 (a) Schematic representation of **DANPY-NO@AuNPs**: AuNPs functionalised with the NO sensitive ligand DANPY-NO-ligand; and (b) normalised extinction spectrum of **DANPY-NO@AuNPs** (DMSO/H_2O (5 : 2), black) and normalised UV-Vis absorption spectrum of DANPY-NO-ligand (DMSO, red).

1.30 μM and a broad dynamic range of detectable concentrations from 0 to 150 μM, an advantage over the molecular probe; good selectivity towards NO over other potential intracellular interferences, and stability at pHs from 3.5 to 8. Biologically, the **DANPY-NO@AuNPs** showed great biocompatibility, and were used to detect and monitor different NO concentrations in mouse macrophages, human macrophages, endothelial cells, and breast cancer cells employing techniques that include CLSM (images and intracellular fluorescence emission spectra), multiphoton microscopy and flow cytometry.

Results and discussion

The novel two-photon excitable nanoprobe, **DANPY-NO@AuNPs** (Fig. 1(a)), consists of a thiolated NO-sensitive ligand (DANPY-NO-ligand) self-assembled onto the surface of AuNPs. The fluorescent NO-sensitive ligand is a derivative of the recently published DANPY-NO[42] and, as such, presents an *o*-phenylenediamine linked to a naphthalimide core, which is responsible for the fluorescence quenching, due to a photoinduced electron transfer (PET), in the absence of NO. Upon reaction with NO in the presence of oxygen, and the consequent formation of the benzotriazole derivative, the PET is suppressed, the quenching effect is diminished, and the fluorescence emission of DANPY-NO-ligand is enhanced.

Synthesis and characterisation of the DANPY-NO@AuNPs

DANPY-NO was chosen as the NO-sensitive two-photon excitable fluorophore due to its high photostability, good sensitivity and excellent selectivity towards NO, its fluorescence stability at different biologically relevant pHs, its excellent biocompatibility and because it is extremely versatile in the detection of NO in cellular environments.[42] Furthermore, the versatile piperazine moiety in DANPY-NO allows the incorporation of a thiolated chain that can be linked onto the surface of AuNPs. The synthesis of DANPY-NO-ligand was accomplished in five steps starting from 4-bromo-1,8-naphthalic anhydride and 2-nitro-*p*-phenylenediamine (Scheme S1, ESI†) yielding the dimeric form of the thiolated monomer attached to the AuNPs. DANPY-NO-ligand and the four intermediates were characterised by ^{1}H-NMR, ^{13}C-NMR, infrared spectroscopy (FTIR) and high-resolution mass spectrometry (HRMS) (see Fig. S1–S8 and "Materials and methods" section in the ESI† for detailed characterisation).

DANPY-NO@AuNPs were synthesised following a method previously reported by Marín *et al.*[64] and exhibited an average size of 2.4 ± 0.7 nm, calculated using transmission electron microscopy (TEM, Fig. S9, ESI†). The **DANPY-NO@AuNPs** exhibited an absorption maximum centred at 401 nm (Fig. 1(b)), evidencing the presence of the DANPY-NO-ligand (absorption maximum at 397 nm in DMSO and molar extinction coefficient of 5.7 × 10^3 M^{-1} cm^{-1} (Fig. S10, ESI†), and a broad background extinction, from 315 to 750 nm, due to the surface plasmon band of the gold core. The successful synthesis of the **DANPY-NO@AuNPs** was further confirmed by recording the fluorescence excitation and emission spectra, which showed similar shapes and maximum wavelengths than those of DANPY-NO-ligand with small shifts in the maximum wavelengths that may be due to the differences in the polarity of the solvents used for the sample preparation (Fig. S11, ESI†). The fluorescence emission spectrum of **DANPY-NO@AuNPs** was also recorded in different biologically relevant media including bovine serum albumin (BSA, 0.1%), Dulbecco's modified Eagle's medium (DMEM) cell culture medium and Hanks' balanced salt solution (HBSS) medium (Fig. S12, ESI†) showing small bathochromic shifts as a consequence of the presence of proteins, inorganic salts, buffering agents, amino acids and vitamins. The synthesis of the **DANPY-NO@AuNPs** was reproducible (Fig. S13, ESI†) and the NPs exhibited excellent stability over time (up to a minimum of 4 months) when stored in aqueous media and at room temperature (Fig. S14, ESI†).

The ability of the **DANPY-NO@AuNPs** to detect NO in solution was evaluated by monitoring changes in the fluorescence emission intensity upon the addition of increasing concentrations of the NO donor NONOate (Fig. S15, ESI†). The nanoprobe showed good sensitivity with a LOD of 1.30 μM,

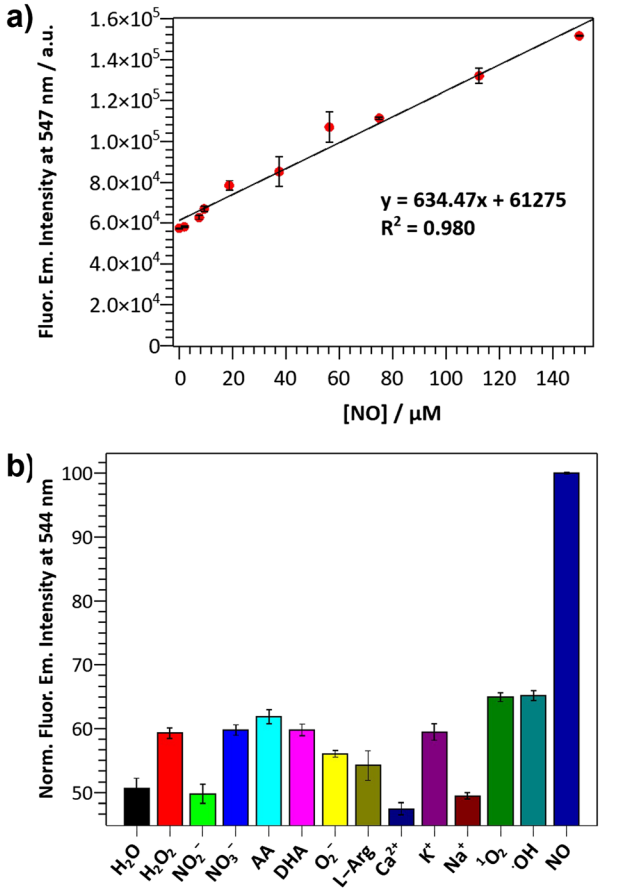

Fig. 2 (a) NO calibration curve of aqueous **DANPY-NO@AuNPs** (83 μg mL^{-1}, 7% DMSO): fluorescence emission intensity at 547 nm as a function of NO concentration; (λ_{exc} = 405 nm); and (b) normalised fluorescence response at 544 nm of aqueous **DANPY-NO@AuNPs** (86 μg mL^{-1}, 7% DMSO) in the presence of NO and various biologically relevant species (100 μM). Each experiment was repeated in triplicate and the relative standard error is indicated by the error bars.

calculated from the linear range in Fig. 2(a), which confirms the suitability of the nanoprobe for monitoring intracellular NO concentrations. Additionally, the nanoprobe was able to detect concentrations of NO up to 150 μM, which is an excellent dynamic range for intracellular levels of NO, especially for cases with elevated concentrations of NO such as bacterial infection. The response time for a fixed concentration of NO was evaluated for a period of 24 h, with a plateau reached *ca.* 10 h following the addition of NONOate (Fig. S16, ESI†). The **DANPY-NO@AuNPs** were stable at biologically relevant pHs (Fig. S17, ESI†) and their fluorescence emission intensity increased slightly at acidic pHs as expected for PET-based systems (Fig. S18, ESI†). **DANPY-NO@AuNPs** were able to detect NO at pH values of biological relevance (pH *ca.* 4.14, 5.63 and 7.30, Fig. S19, ESI†), demonstrating the potential of the nanoprobe to detect NO in the different intracellular organelles including those with low pH.

The selectivity of **DANPY-NO@AuNPs** towards NO was examined in solution showing a considerable increase in fluorescence emission intensity in the presence of NO while negligible or small changes were observed in the presence of ROS and RNS species (100 μM, H_2O_2, O_2^-, $^{\bullet}OH$, $^1O_2$, NO_2^- and NO_3^-) and other possible cellular interferences (100 μM, Na^+, K^+, Ca^{2+}, L-arginine (L-Arg), ascorbic acid (AA) and dehydroascorbic acid (DHA)) (Fig. 2(b)). These results suggest that the nanoprobe is more selective towards NO. Additionally, the **DANPY-NO@AuNPs** were still able to detect NO in the presence of the tested interferents (Fig. S20, ESI†).

Intracellular characterisation of DANPY-NO@AuNPs and nitric oxide detection in RAW264.7γ NO^-

The internalisation of **DANPY-NO@AuNPs** in live cells was investigated using RAW264.7γ NO^- macrophages. CLSM fluorescence images of the cells incubated with **DANPY-NO@AuNPs** showed a brighter fluorescence emission, indicating the presence of the nanoprobe in the cells, compared to those cells that were not incubated with the **DANPY-NO@AuNPs** (Fig. 3(a)). To confirm that the observed fluorescence was due to the internalised **DANPY-NO@AuNPs**, the fluorescence emission spectrum of the cells was recorded using the CLSM showing an emission band from 430 to 630 nm with a maximum intensity at *ca.* 511 nm (red in Fig. 3(b)), which was comparable to that of **DANPY-NO@AuNPs** in DMEM cell culture medium recorded in the spectrophotometer (black in Fig. 3(b)). Both spectra exhibited the shape characteristic of a naphthalimide-based fluorophore and the 16 nm difference in the maximum wavelength can be attributed to the complexity of the cellular environment (differences in polarity, pH, protein binding, among other factors) compared to the DMEM cell culture medium. The fluorescence emission spectrum of control cells without **DANPY-NO@AuNPs** (green in Fig. 3(b)) showed a much lower intensity, which is due to the autofluorescence of the imaged cells.

Most of the studies in the literature report the uptake of NPs by mammalian cells *via* endocytosis in which the NPs are captured at the cell surface and enclosed in invaginations of the cell membrane that ultimately pinch off to form intracellular vesicles.[66] Following endocytosis, the NP-containing vesicles are normally delivered to the lysosomes and thus accumulate in phagolysosomes. To study whether the **DANPY-NO@AuNPs** accumulated in the lysosomes of the RAW264.7γ NO^- cells, LysoTracker™ Red DND-99 was used as marker of acidic organelles. Cells incubated with **DANPY-NO@AuNPs** and LysoTracker™ Red DND-99 were imaged using the CLSM (Fig. 3(c)) showing a clear overlap between the fluorescence emission of the green channel, **DANPY-NO@AuNPs**, and the emission from the red channel, LysoTracker™ Red DND-99, as observed from the yellow spots in the merged image of both channels and the differential interference contrast (DIC). The Pearson's coefficient was calculated to be 0.73 ± 0.04 (n = 3 images, *ca.* 20 cells), further indicating good colocalisation between the **DANPY-NO@AuNPs** and the labelled acidic organelles. The cytotoxicity of **DANPY-NO@AuNPs** in RAW264.7γ NO^- cells, determined using the CellTiter-Blue® cell viability assay, showed an excellent cell survival rate at concentrations tested up to 4.2 μg mL^{-1}, which is the concentration used in the intracellular experiments (Fig. S21, ESI†).

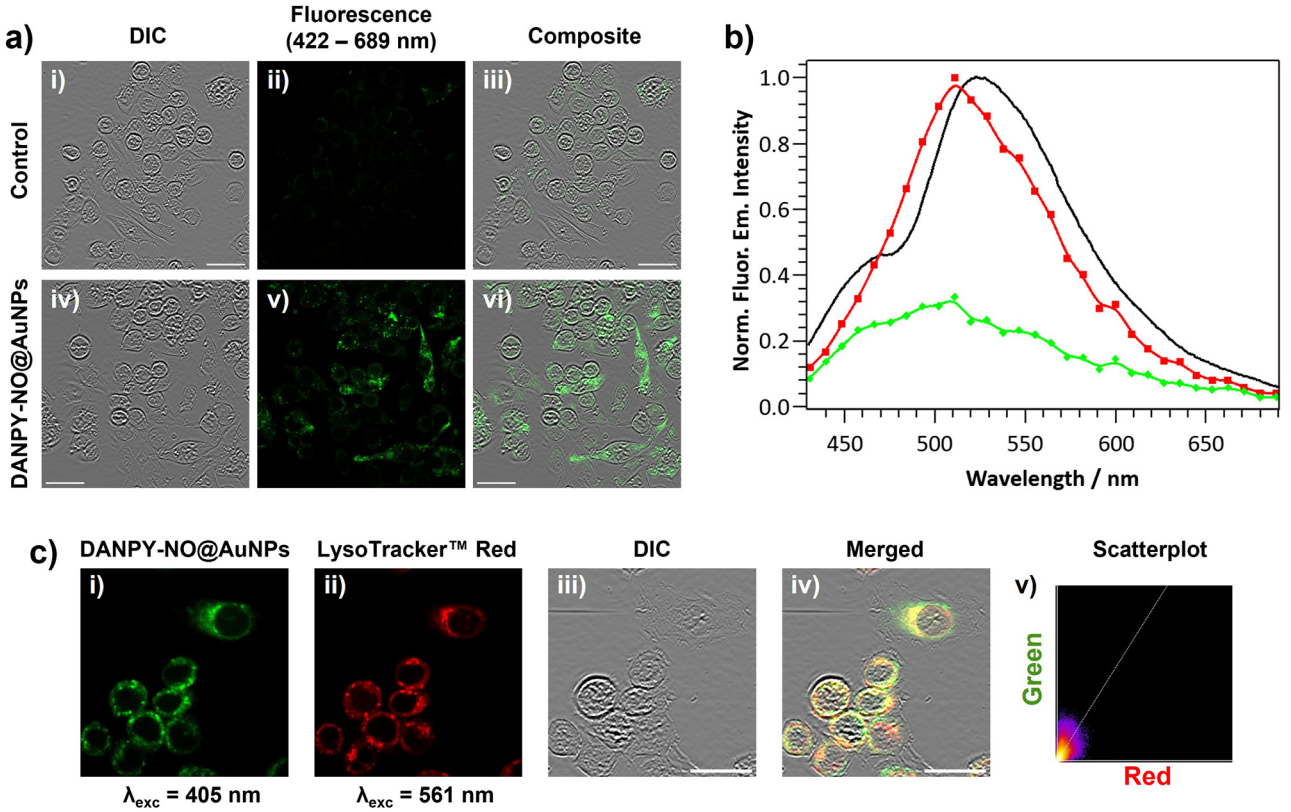

Fig. 3 (a) CLSM images of RAW264.7γ NO^- cells untreated (i)–(iii) and incubated with **DANPY-NO@AuNPs** (4.2 μg mL^{-1}, overnight) (iv)–(vi); images collected using λ_{exc} = 405 nm and $\Delta\lambda_{em}$ = 422–689 nm. Scale bars = 25 μm. (b) Normalised fluorescence emission spectrum of: **DANPY-NO@AuNPs** in DMEM cell culture medium recorded in the fluorescence spectrophotometer (black); RAW264.7γ NO^- cells incubated with **DANPY-NO@AuNPs** recorded in the CLSM (red); and control cells without **DANPY-NO@AuNPs** loaded recorded in the CLSM (green); λ_{exc} = 405 nm. (c) CLSM images of RAW264.7γ NO^- cells incubated with **DANPY-NO@AuNPs** (4.2 μg mL^{-1}) and LysoTracker™ Red DND-99 (5 μM) (i)–(iv) and scatterplot showing the correlation between the green and red emission intensities (v). Images collected upon excitation at (i) λ_{exc} = 405 nm, $\Delta\lambda_{em}$ = 500–580 nm and (ii) λ_{exc} = 561 nm, $\Delta\lambda_{em}$ = 580–625 nm; (iii) DIC channel; and (iv) composite image of green, red and DIC channels. Pearson's coefficient of 0.73 ± 0.04 (*n* = 3 images, *ca.* 20 cells). Scale bars = 20 μm.

The **DANPY-NO@AuNPs** were used to intracellularly detect endogenous NO concentrations produced by RAW264.7γ NO^- cells when stimulated with lipopolysaccharide (LPS) and interferon-gamma (IFN-γ). CLSM images of stimulated cells that had been incubated with **DANPY-NO@AuNPs** exhibited an intense fluorescence emission intensity compared to unstimulated cells that had been also incubated with the nanoprobe (Fig. 4(a)). Stimulated and unstimulated control cells without **DANPY-NO@AuNPs** did not show any evident fluorescence emission (Fig. S22, ESI†). The enhancement of the fluorescence emission intensity upon stimulation confirmed the successful performance of the **DANPY-NO@AuNPs** in the detection of endogenous intracellular NO. The results obtained from the CLSM images were further supported by recording the fluorescence emission spectra of the cells using the CLSM (Fig. 4(b)). An enhancement of the fluorescence emission intensity of the cells incubated with **DANPY-NO@AuNPs** was observed upon stimulation to produce NO (from black to green in Fig. 4(b)). Importantly, the fluorescence emission spectra of unstimulated and stimulated cells without **DANPY-NO@AuNPs** (blue and yellow, respectively) showed a negligible intensity in comparison to the cells incubated with the nanoprobe.

To study the selective intracellular detection of NO by **DANPY-NO@AuNPs**, RAW264.7γ NO^- cells were pre-treated with (ω)-nitro-L-arginine methyl ester (L-NAME), an inhibitor of nitric oxide synthase (NOS) which blocks the production of NO, stimulated overnight with LPS and IFN-γ and then incubated with **DANPY-NO@AuNPs** for 3 h before imaging. The fluorescence emission spectrum of these treated cells showed an intensity comparable to that of unstimulated cells (Fig. 4(b), red) confirming the selectivity of the **DANPY-NO@AuNPs** towards NO (corresponding CLSM images are shown in Fig. S23, ESI†). To further investigate the potential of **DANPY-NO@AuNPs**, their ability to detect NO in a large population of cells was evaluated using flow cytometry (Fig. 5(a)). The internalisation of the nanoprobe by the cells was evidenced by the clear difference between the mean fluorescence intensity of unstimulated cells incubated with **DANPY-NO@AuNPs** (134 ± 3 a.u.) and that of unstimulated or stimulated cells without **DANPY-NO@AuNPs** (72 ± 2 a.u. and 89 ± 5 a.u., respectively). Importantly, a higher mean fluorescence intensity was observed for the stimulated cells incubated with the nanoprobe (181 ± 16 a.u.) when compared to the unstimulated cells.

Given the excellent performance of **DANPY-NO@AuNPs** for the detection of intracellularly produced NO under one-photon

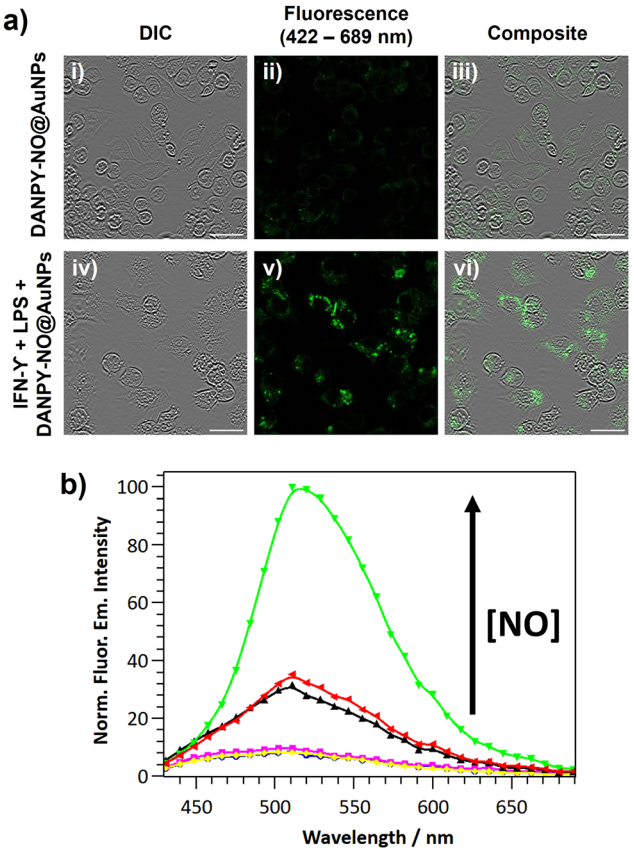

Fig. 4 (a) CLSM images of unstimulated (i)–(iii) and stimulated (iv)–(vi) RAW264.7γ NO^- cells both incubated overnight with **DANPY-NO@AuNPs**. (b) Normalised fluorescence emission spectrum of: cells incubated with **DANPY-NO@AuNPs** unstimulated (black), stimulated (green) and pre-incubated with L-NAME and stimulated (red); and control cells without **DANPY-NO@AuNPs** under the previous conditions, blue, yellow and magenta, respectively. Incubation with **DANPY-NO@AuNPs** (4.2 μg mL^{-1}) was done for 3 h. Stimulation was performed overnight using LPS (0.7 μg mL^{-1}) and IFN-γ (17 μg mL^{-1}) and the pre-treatment with L-NAME (2 mM) was done for 30 min. λ_{exc} = 405 nm and $\Delta\lambda_{em}$ = 422–689 nm. Scale bars = 25 μm.

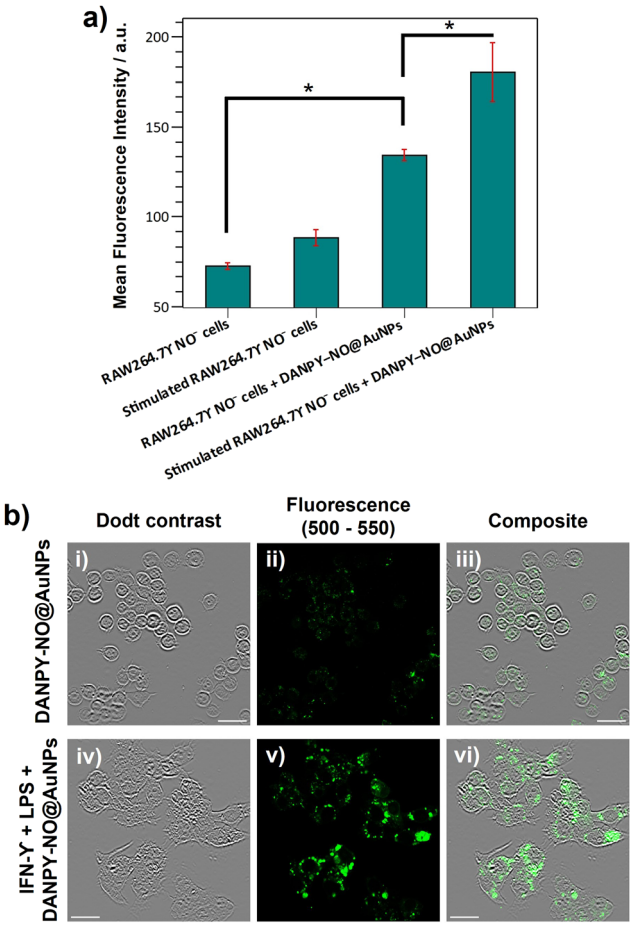

Fig. 5 (a) Flow cytometry assay for **DANPY-NO@AuNPs** in RAW264.7γ NO^- cells. Control cells and cells incubated with **DANPY-NO@AuNPs** (4.2 μg mL^{-1}, overnight): unstimulated and stimulated. Stimulation was performed overnight using LPS (0.7 μg mL^{-1}) and IFN-γ (17 μg mL^{-1}). λ_{exc} = 405 nm and $\Delta\lambda_{em}$ = 500–550 nm. Approximately 10 000 cells were analysed for each sample. Each experiment was repeated in triplicate and the relative standard error is indicated by the error bars. * Represents a statistically significant difference of $p < 0.05$ (Student's *t* test) comparing both measurements. (b) Multiphoton microscopy images of unstimulated (i)–(iii) and stimulated (iv)–(vi) RAW264.7γ NO^- cells incubated with **DANPY-NO@AuNPs** (4.2 μg mL^{-1}, overnight); λ_{exc} = 800 nm and $\Delta\lambda_{em}$ = 500–550 nm. Scale bars = 25 μm.

excitation (405 nm), the ability of the nanoprobe to be excited by two-photon excitation (800 nm), and to be used to monitor intracellular NO production under these excitation conditions was investigated in a multiphoton microscope (Fig. 5(b)). Cells incubated with **DANPY-NO@AuNPs** showed a green fluorescence emission intensity that increased upon stimulation; while control cells did not show measurable fluorescence (Fig. S24, ESI†). These results proved the ability of the nanoprobe to be NIR excitable *via* two-photon excitation and its potential application to monitor intracellular NO levels using a multiphoton microscope.

Nitric oxide detection in THP-1 human macrophages using DANPY-NO@AuNPs

To further study the application of **DANPY-NO@AuNPs** in cellular environments and their potential to monitor low levels of NO, THP-1 human macrophages, which are known to produce nanomolar concentrations of NO, were chosen as the next biological target. The internalisation of the **DANPY-NO@AuNPs** within THP-1 macrophages was successfully proven using CLSM, and their colocalisation with LysoTracker™ Red DND-99 was demonstrated with a Pearson's coefficient of 0.67 ± 0.04 (n = 3 images, *ca.* 15 cells) (Fig. S25, ESI†). The cell viability results obtained for the concentrations of **DANPY-NO@AuNPs** tested showed a cell survival above 80% for concentrations up to 4.2 μg mL^{-1} (Fig. S26, ESI†), demonstrating the low toxicity of the nanoprobe in THP-1 cells. The intracellular detection of NO in THP-1 differentiated macrophages using **DANPY-NO@AuNPs** was investigated by recording CLSM images (Fig. S27, ESI†) and, importantly, by recording the fluorescence emission spectra of the imaged cells (Fig. 6). Cells incubated with the nanoprobe and stimulated to produce NO showed a higher fluorescence emission intensity (green) than

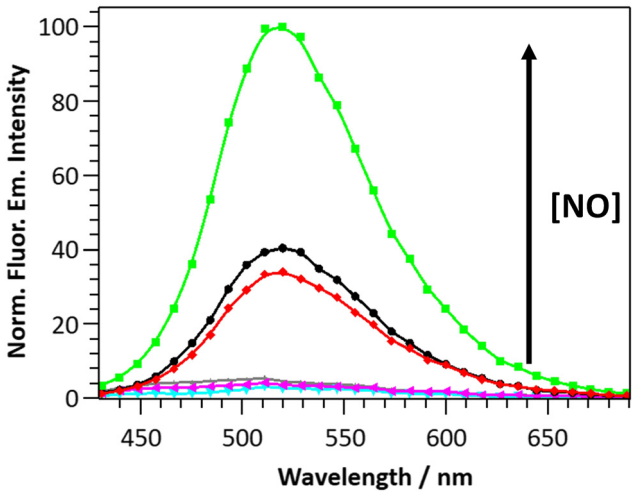

Fig. 6 Normalised fluorescence emission spectra of unstimulated (black), stimulated (green), and pre-treated with L-NAME and stimulated (red) THP-1 macrophages incubated overnight with **DANPY-NO@AuNPs** (4.2 μg mL^{-1}). Grey, cyan and magenta emission spectra correspond to the control cells without **DANPY-NO@AuNPs** under the previous conditions, respectively. Stimulation was performed overnight with LPS (5 μg mL^{-1}) and treatment with L-NAME (0.1 mM) was done 30 min before stimulation. λ_{exc} = 405 nm and $\Delta\lambda_{em}$ = 422–689 nm.

the unstimulated cells incubated with **DANPY-NO@AuNPs** (black), proving the successful detection of NO endogenously produced by THP-1 macrophages. Fluorescence images and corresponding emission spectra of control cells without **DANPY-NO@AuNPs**, both stimulated (grey) and unstimulated (cyan), showed negligible fluorescence upon excitation at 405 nm. Furthermore, pre-treatment of the THP-1 cells with L-NAME and consequent inhibition of the NO production by inducible NOS (iNOS) confirmed the selectivity of the **DANPY-NO@AuNPs** towards intracellular NO (Fig. 6 – red).

Nitric oxide detection in endothelial cells using DANPY-NO@AuNPs

DANPY-NO@AuNPs were also internalised by endothelial cells where they accumulated in the acidic organelles (Fig. S28, ESI†) showing negligible toxicity (Fig. S29, ESI†). To investigate the ability of the **DANPY-NO@AuNPs** to detect endogenous NO produced by endothelial cells, a comparative study between the concentration of NO in basal conditions, upon treatment with Ca^{2+} ionophore A-23187 to enhance the production of NO (since endothelial NOS (eNOS) is a Ca^{2+} dependent enzyme), and after inhibition of the eNOS using L-NAME was performed (Fig. 7(a) for images and Fig. 7(b) for corresponding spectra). The corresponding control cells without **DANPY-NO@AuNPs** were also imaged using the CLSM (Fig. S30 for images, ESI† and Fig. 7(b) for corresponding spectra). Cells incubated with **DANPY-NO@AuNPs** and treated with Ca^{2+} ionophore A-23187 showed a higher fluorescence emission intensity (purple) compared to those cells incubated only with the nanoprobe (black) indicating the successful detection of endogenous NO produced by endothelial cells. Contrarily, when the cells were incubated with **DANPY-NO@AuNPs** and L-NAME, a clear reduction of the

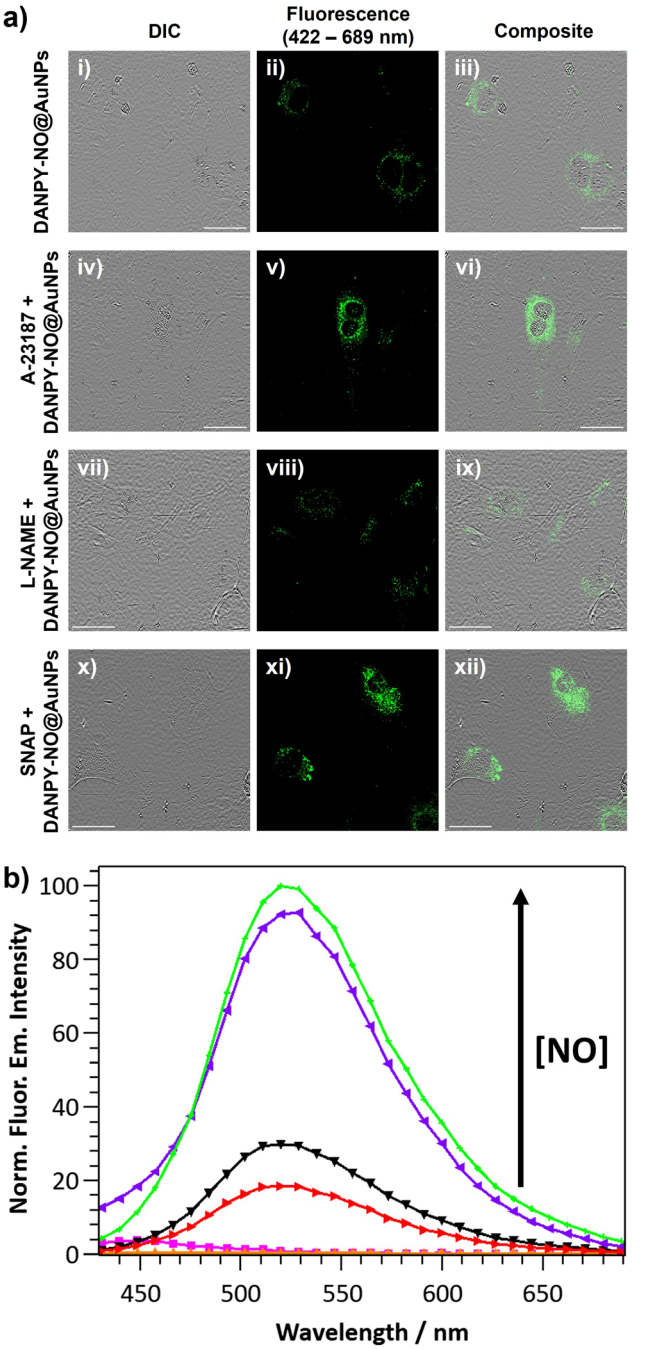

Fig. 7 (a) CLSM images of untreated (i)–(iii), treated with Ca^{2+} ionophore A-23187 (iv)–(vi), treated with L-NAME (vii)–(ix) and treated with SNAP (x)–(xii) endothelial cells all incubated overnight with **DANPY-NO@AuNPs** (4.2 μg mL^{-1}). Scale bars = 50 μm. (b) The corresponding normalised fluorescence emission spectra. Black, purple, red and green emission spectra correspond to cells incubated with **DANPY-NO@AuNPs** and untreated, treated with Ca^{2+} ionophore A-23187, treated with L-NAME and treated with SNAP, respectively. Cyan, magenta, yellow and orange emission spectra correspond to the corresponding control cells without **DANPY-NO@AuNPs**. Treatments with Ca^{2+} ionophore A-23187 (1 μM), with L-NAME (200 mM) and with SNAP (220 μM) were performed overnight. λ_{exc} = 405 nm and $\Delta\lambda_{em}$ = 422–689 nm.

emission intensity was observed (red), which was slightly lower than that of cells incubated only with **DANPY-NO@AuNPs**,

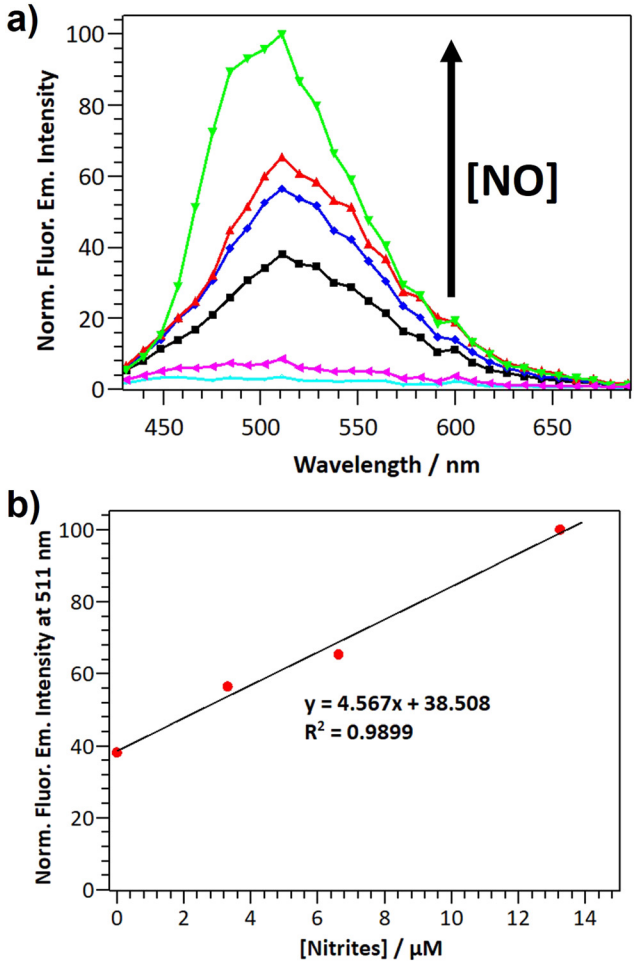

Fig. 8 (a) Normalised fluorescence emission (λ_{exc} = 405 nm) spectra of MDA-MB-231 cells incubated overnight with **DANPY-NO@AuNPs** (4.2 μg mL^{-1}) untreated (black) and treated with different concentrations of SNAP: 110 μM (blue), 220 μM (red) and 440 μM (green); and (b) corresponding linear adjustment of the normalised fluorescence emission intensity at 511 nm as a function of nitrites concentration. Fluorescence emission spectra of control cells incubated without **DANPY-NO@AuNPs** and treated with (pink) and without (cyan) SNAP were also recorded.

demonstrating the successful inhibition of the eNOS and the selective detection of NO by our nanoprobe. Additionally, the ability of the nanoprobe to also detect exogenous NO levels was confirmed using *S*-nitroso-*N*-acetylpenicillamine (SNAP) as a NO donor. Images of cells treated with SNAP exhibited an enhanced green intensity compared to cells only treated with the nanoprobe (from Fig. 7(a)-(ii)–(xi)); and the corresponding fluorescence emission spectra (green for cells treated with SNAP and black for cells only incubated with the **DANPY-NO@AuNPs**) corroborate the results. It is important to notice that the fluorescence emission spectrum of cells incubated with Ca^{2+} ionophore A-23187 showed a small shoulder at 440 nm, which is attributed to the fluorescence emission of this compound. These results confirmed the ability of **DANPY-NO@AuNPs** to detect endogenous NO concentrations in endothelial cells, which are produced at nanomolar concentrations, and the possibility of monitoring the presence of exogenous NO produced by a NO donor.

Nitric oxide detection in breast cancer cells using DANPY-NO@AuNPs

The potential application of **DANPY-NO@AuNPs** to quantify intracellular NO concentrations was explored in MDA-MB-231 breast cancer cells. Cells incubated overnight with **DANPY-NO@AuNPs** and treated with different concentrations of the NO donor SNAP (from 0 to 440 μM) showed green emission which increased in intensity with a concomitant increase in SNAP concentrations (Fig. S31, ESI†). The CLSM images were supported with the fluorescence emission spectra of all the samples (Fig. 8(a)). Control cells without **DANPY-NO@AuNPs**, both treated and untreated with SNAP, did not show the characteristic fluorescence emission of the **DANPY-NO@AuNPs**. The results showed a clear enhancement of the fluorescence emission intensity of the cells containing **DANPY-NO@AuNPs** that was associated with the concentration of SNAP, and therefore with the concentration of NO released in each sample. The fluorescence emission intensity at 511 nm for each sample was plotted as a function of the concentration of nitrites and a linear adjustment was obtained (Fig. 8(b)) showing a good correlation between the fluorescence emission signal of the **DANPY-NO@AuNPs** and the concentration of nitrites released in the cells. This calibration curve could be potentially used for the quantification of NO concentrations present in unknown samples.

Conclusions

In summary, we have reported a two-photon fluorescent nanoprobe, **DANPY-NO@AuNPs**, able to detect NO produced by iNOS and eNOS in a wide selection of cells, and with potential to intracellularly quantify NO. The synthesis of **DANPY-NO@AuNPs** was reproducible and the resulting AuNPs were stable for at least four months after the synthesis. In solution, the **DANPY-NO@AuNPs** showed good sensitivity towards NO with a LOD of 1.30 μM and with a dynamic range of detectable concentrations from 0 to 150 μM; both excellent characteristics for the intracellular detection of NO. The **DANPY-NO@AuNPs** presented good selectivity towards NO over other potential intracellular interferences including ROS and RNS. Additionally, **DANPY-NO@AuNPs** were stable and able to detect NO at biologically relevant pHs. The nanoprobe exhibited great biological potential and versatility. The **DANPY-NO@AuNPs**, which exhibited negligible cytotoxicity, were used to detect and monitor different NO concentrations in mouse macrophages (RAW264.7γ NO^- cells), human macrophages (THP-1 cells), endothelial cells and breast cancer cells (MDA-MB-231 cells). Importantly, a calibration curve that can potentially be used to quantify intracellular NO concentrations was obtained by measuring exogenous NO in cancer cells. The **DANPY-NO@AuNPs** exhibited excellent versatility for the detection of intracellular NO as it has been confirmed when using a range of techniques including CLSM (images and intracellular fluorescence emission spectra), multiphoton microscopy and flow cytometry. Overall, due to their reproducibility, stability, sensitivity, selectively, biological versatility and biocompatibility, **DANPY-NO@AuNPs** have

proven to be an excellent tool to monitor and potentially quantify intracellular NO *in vitro* and their ability to be two-photon excitable makes them extremely valuable to aid our further understanding of the role that NO plays in biology, investigating 3D models and *in vivo* models. Although **DANPY-NO@AuNPs** exhibit a higher LOD than the recently published DANPY-NO molecular probe,[42] the nanoprobe exhibits a set of characteristics that make **DANPY-NO@AuNPs** excellent candidates for biomedical applications: (1) the broader dynamic range of the nanoprobe permits its application in biological samples with elevated concentrations of NO such as in the case of bacterial infection; (2) **DANPY-NO@AuNPs** have proven to be more stable in aqueous media compared to the molecular probe; and (3) importantly, having a nanoplatform permits the incorporation of other ligands such as reference ligands to obtain ratiometric nanoprobes for the precise quantification of intracellular NO, or drugs yielding nanoplatforms for theranostic applications.

Author contributions

C. A. V. performed all the experimental work described in this paper and analysed the data, wrote the original draft of the manuscript and the ESI† and contributed to the later reviewing and editing. P. T. provided training and supervision of the imaging techniques and contributed to reviewing and editing the manuscript. F. G. contributed to the design of the project and reviewing the manuscript. M. P. M. provided training and supervision of the synthesis of DANPY-NO-ligand and contributed to writing, reviewing and editing the manuscript. M. J. M. supervised the entire research with conceptualisation, analysis and resources, contributed to the writing, and coordinated the reviewing and editing of the final manuscript. All authors have given approval to the final manuscript.

Conflicts of interest

The authors declare that they have no known competing financial interests or personal relationships that could have appeared to influence the work reported in this paper.

Acknowledgements

The authors acknowledge Dr Derek Warren and Dr Anastasia Sobolewski (School of Pharmacy, University of East Anglia) for kindly providing the endothelial cells and THP-1 cells, respectively. The authors acknowledge Dr Andrew Goldson for training and guidance on the flow cytometer; Dr Philip Wilson for training and guidance on the multiphoton microscope. The authors would like to thank the Faculty of Sciences and School of Chemistry at the University of East Anglia, and Mr and Mrs Whittaker oncology fellowship for financial support; and the EPSRC (grant EP/S017909/1) that supported the purchase of the Edinburgh Instrument FS5 fluorescence spectrometer used in this work.

Notes and references

1 D. Mishra, V. Patel and D. Banerjee, *Breast Cancer*, 2020, **14**, 1178223419882688.
2 C. Yu, Y. Wu, F. Zeng and S. Wu, *J. Mater. Chem. B*, 2013, **1**, 4152–4159.
3 L. L. Thomsen, D. W. Miles, L. Happerfield, L. G. Bobrow, R. G. Knowles and S. Moncada, *Br. J. Cancer*, 1995, **72**, 41–44.
4 O. Gallo, E. Masini, L. Morbidelli, A. Franchi, I. Fini-Storchi, W. A. Vergari and M. Ziche, *J. Natl. Cancer Inst.*, 1998, **90**, 587–596.
5 S. Ambs, W. G. Merriam, W. P. Bennett, E. Felley-Bosco, M. O. Ogunfusika, S. M. Oser, S. Klein, P. G. Shields, T. R. Billiar and C. C. Harris, *Cancer Res.*, 1998, **58**, 334–341.
6 A. Erlandsson, J. Carlsson, S. O. Andersson, C. Vyas, P. Wikström, O. Andrén, S. Davidsson and J. R. Rider, *Scand. J. Urol.*, 2018, **52**, 129–133.
7 H. Cheng, L. Wang, M. Mollica, A. T. Re, S. Wu and L. Zuo, *Cancer Lett.*, 2014, **353**, 1–7.
8 E. Eroglu, S. Charoensin, H. Bischof, J. Ramadani, B. Gottschalk, M. R. Depaoli, M. Waldeck-Weiermair, W. F. Graier and R. Malli, *Free Radical Biol. Med.*, 2018, **128**, 50–58.
9 E. Goshi, G. Zhou and Q. He, *Med. Gas Res.*, 2019, **9**, 192–207.
10 C. Csonka, T. Páli, P. Bencsik, A. Görbe, P. Ferdinandy and T. Csont, *Br. J. Pharmacol.*, 2015, **172**, 1620–1632.
11 Y. Chen, *Nitric oxide*, 2020, **98**, 1–19.
12 T. Nagano and T. Yoshimura, *Chem. Rev.*, 2002, **102**, 1235–1270.
13 H. Li, Y.-H. Hao, W. Feng and Q.-H. Song, *J. Mater. Chem. B*, 2020, **8**, 9785–9793.
14 S. Ma, X. Sun, Q. Yu, R. Liu, Z. Lu and L. He, *Photochem. Photobiol. Sci.*, 2020, **19**, 1230–1235.
15 Q. Han, J. Liu, Q. Meng, Y.-L. Wang, H. Feng, Z. Zhang, Z. P. Xu and R. Zhang, *ACS Sens.*, 2019, **4**, 309–316.
16 W.-L. Jiang, Y. Li, H.-W. Liu, D.-Y. Zhou, J. Ou-Yang, L. Yi and C.-Y. Li, *Talanta*, 2019, **197**, 436–443.
17 Y. Yu, X. Zhang, Y. Dong, X. Luo, X. Qian and Y. Yang, *Sens. Actuators, B*, 2021, **346**, 130562.
18 L. Wang, J. Zhang, X. An and H. Duan, *Org. Biomol. Chem.*, 2020, **18**, 1522–1549.
19 A. Beltran, M. Isabel Burguete, D. R. Abanades, D. Perez-Sala, S. V. Luis and F. Galindo, *Chem. Commun.*, 2014, **50**, 3579–3581.
20 I. Muñoz Resta, B. Bedrina, E. Martínez-Planes, A. Minguela and F. Galindo, *J. Mater. Chem. B*, 2021, **9**, 9885–9892.
21 E. M. Hetrick and M. H. Schoenfisch, *Annu. Rev. Anal. Chem.*, 2009, **2**, 409–433.
22 M. J. Marín, P. Thomas, V. Fabregat, S. V. Luis, D. A. Russell and F. Galindo, *ChemBioChem*, 2011, **12**, 2471–2477.
23 H. Kojima, N. Nakatsubo, K. Kikuchi, S. Kawahara, Y. Kirino, H. Nagoshi, Y. Hirata and T. Nagano, *Anal. Chem.*, 1998, **70**, 2446–2453.
24 H. Kojima, K. Sakurai, K. Kikuchi, S. Kawahara, Y. Kirino, H. Nagoshi, Y. Hirata and T. Nagano, *Chem. Pharm. Bull.*, 1998, **46**, 373–375.

25 H. Kojima, Y. Urano, K. Kikuchi, T. Higuchi, Y. Hirata and T. Nagano, *Angew. Chem., Int. Ed.*, 1999, **38**, 3209–3212.
26 H. Kojima, M. Hirotani, N. Nakatsubo, K. Kikuchi, Y. Urano, T. Higuchi, Y. Hirata and T. Nagano, *Anal. Chem.*, 2001, **73**, 1967–1973.
27 Y. Gabe, Y. Urano, K. Kikuchi, H. Kojima and T. Nagano, *J. Am. Chem. Soc.*, 2004, **126**, 3357–3367.
28 E. Sasaki, H. Kojima, H. Nishimatsu, Y. Urano, K. Kikuchi, Y. Hirata and T. Nagano, *J. Am. Chem. Soc.*, 2005, **127**, 3684–3685.
29 R. Zhang, Z. Ye, G. Wang, W. Zhang and J. Yuan, *Chem. – Eur. J.*, 2010, **16**, 6884–6891.
30 A. K. Vidanapathirana, J. M. Goyne, A. E. Williamson, B. J. Pullen, P. Chhay, L. Sandeman, J. Bensalem, T. J. Sargeant, R. Grose, M. J. Crabtree, R. Zhang, S. J. Nicholls, P. J. Psaltis and C. A. Bursill, *Biomedicines*, 2022, **10**, 1807.
31 D. Kim, H. G. Ryu and K. H. Ahn, *Org. Biomol. Chem.*, 2014, **12**, 4550–4566.
32 R. K. P. Benninger and D. W. Piston, *Curr. Protoc. Cell Biol.*, 2013, **59**, 4.11.1–4.11.24.
33 E. W. Seo, J. H. Han, C. H. Heo, J. H. Shin, H. M. Kim and B. R. Cho, *Chem. – Eur. J.*, 2012, **18**, 12388–12394.
34 X. Dong, C. H. Heo, S. Chen, H. M. Kim and Z. Liu, *Anal. Chem.*, 2014, **86**, 308–311.
35 Z. Mao, W. Feng, Z. Li, L. Zeng, W. Lv and Z. Liu, *Chem. Sci.*, 2016, **7**, 5230–5235.
36 M. Wang, Z. Xu, X. Wang and J. Cui, *Dyes Pigm.*, 2013, **96**, 333–337.
37 C.-B. Huang, J. Huang and L. Xu, *RSC Adv.*, 2015, **5**, 13307–13310.
38 H. Yu, Y. Xiao and L. Jin, *J. Am. Chem. Soc.*, 2012, **134**, 17486–17489.
39 W. Feng, Q.-L. Qiao, S. Leng, L. Miao, W.-T. Yin, L.-Q. Wang and Z.-C. Xu, *Chin. Chem. Lett.*, 2016, **27**, 1554–1558.
40 N. Gupta, S. Imam Reja, V. Bhalla, M. Gupta, G. Kaur and M. Kumar, *Chem. – Asian J.*, 2016, **11**, 1020–1027.
41 S.-J. Li, D.-Y. Zhou, Y. Li, H.-W. Liu, P. Wu, J. Ou-Yang, W.-L. Jiang and C.-Y. Li, *ACS Sens.*, 2018, **3**, 2311–2319.
42 C. Arnau del Valle, L. Williams, P. Thomas, R. Johnson, S. Raveenthiraraj, D. Warren, A. Sobolewski, M. P. Muñoz, F. Galindo and M. J. Marín, *J. Photochem. Photobiol., B*, 2022, **234**, 112512.
43 Y. E. Lee, R. Smith and R. Kopelman, *Annu. Rev. Anal. Chem.*, 2009, **2**, 57–76.
44 P. Jin, C. Wiraja, J. Zhao, J. Zhang, L. Zheng and C. Xu, *ACS Appl. Mater. Interfaces*, 2017, **9**, 25128–25137.
45 D. Yeo, C. Wiraja, Y. J. Chuah, Y. Gao and C. Xu, *Sci. Rep.*, 2015, **5**, 14768.
46 G. Zhang, F. P. Shu and C. J. Robinson, *Annu. Int. Conf. IEEE Eng. Med. Biol. Soc.*, 2007, vol. 2007, pp. 103–106.
47 A. V. Latha, M. Ayyappan, A. R. Kallar, R. V. Kakkadavath, S. P. Victor and S. Selvam, *Mater. Sci. Eng., C*, 2020, **108**, 110463.
48 S. Bhattacharya, R. Sarkar, B. Chakraborty, A. Porgador and R. Jelinek, *ACS Sens.*, 2017, **2**, 1215–1224.
49 L. Tan, A. Wan, H. Li, H. Zhang and Q. Lu, *Mater. Chem. Phys.*, 2012, **134**, 562–566.
50 C.-H. Quek and K. W. Leong, *Nanomaterials*, 2012, **2**, 92–112.
51 X. He, J. Gao, S. S. Gambhir and Z. Cheng, *Trends Mol. Med.*, 2010, **16**, 574–583.
52 J.-H. Kim, D. A. Heller, H. Jin, P. W. Barone, C. Song, J. Zhang, L. J. Trudel, G. N. Wogan, S. R. Tannenbaum and M. S. Strano, *Nat. Chem.*, 2009, **1**, 473–481.
53 H. Wang, Y. Liu, Z. Wang, M. Yang and Y. Gu, *Nanoscale*, 2018, **10**, 10641–10649.
54 F. Bai, W. Du, X. Liu, L. Su, Z. Li, T. Chen, X. Ge, Q. Li, H. Yang and J. Song, *Anal. Chem.*, 2021, **93**, 15279–15287.
55 J. R. G. Navarro and F. Lerouge, *Nanophotonics*, 2017, **6**, 71.
56 S. Zeng, K.-T. Yong, I. Roy, X.-Q. Dinh, X. Yu and F. Luan, *Plasmonics*, 2011, **6**, 491.
57 Y. Peng, L. Qin, S.-Z. Kang, G. Li and X. Li, *Talanta*, 2019, **191**, 457–460.
58 R. Leggett, P. Thomas, M. J. Marín, J. Gavrilovic and D. A. Russell, *Analyst*, 2017, **142**, 4099–4105.
59 R. A. Sperling, P. Rivera Gil, F. Zhang, M. Zanella and W. J. Parak, *Chem. Soc. Rev.*, 2008, **37**, 1896–1908.
60 K. Saha, S. S. Agasti, C. Kim, X. Li and V. M. Rotello, *Chem. Rev.*, 2012, **112**, 2739–2779.
61 D. Wang, M. Zhou, H. Huang, L. Ruan, H. Lu, J. Zhang, J. Chen, J. Gao, Z. Chai and Y. Hu, *ACS Appl. Bio Mater.*, 2019, **2**, 3178–3182.
62 P. Rivera_Gil, C. Vazquez-Vazquez, V. Giannini, M. P. Callao, W. J. Parak, M. A. Correa-Duarte and R. A. Alvarez-Puebla, *Angew. Chem., Int. Ed.*, 2013, **52**, 13694–13698.
63 J. Cui, K. Hu, J.-J. Sun, L.-L. Qu and D.-W. Li, *Biosens. Bioelectron.*, 2016, **85**, 324–330.
64 M. J. Marín, F. Galindo, P. Thomas and D. A. Russell, *Angew. Chem., Int. Ed.*, 2012, **51**, 9657–9661.
65 M. J. Marín, F. Galindo, P. Thomas, T. Wileman and D. A. Russell, *Anal. Bioanal. Chem.*, 2013, **405**, 6197–6207.
66 T.-G. Iversen, T. Skotland and K. Sandvig, *Nano Today*, 2011, **6**, 176–185.

